Research Article

Graphene Nanoribbon Grids of Sub-10 nm Widths with High Electrical Connectivity

Namjo Kim,[||] Shinyoung Choi,[||] Seong-Jun Yang, Jewook Park, Jun-Ho Park, Nguyen Ngan Nguyen, Kwanghee Park, Sunmin Ryu, Kilwon Cho, and Cheol-Joo Kim*

Cite This: ACS Appl. Mater. Interfaces 2021, 13, 28593−28599 | Read Online

ACCESS | Metrics & More | Article Recommendations | Supporting Information

ABSTRACT: Quasi-one-dimensional (1D) graphene nanoribbons (GNRs) have finite band gaps and active edge states and therefore can be useful for advanced chemical and electronic devices. Here, we present the formation of GNR grids via seed-assisted chemical vapor deposition on Ge(100) substrates. Nucleation seeds, provided by unzipped C_{60}, initiated growth of the GNRs. The GNRs grew toward two orthogonal directions in an anisotropic manner, templated by the single crystalline substrate, thereby forming grids that had lateral stitching over centimeter scales. The spatially uniform grid can be transferred and patterned for batch fabrication of devices. The GNR grids showed percolative conduction with a high electrical sheet conductance of ~2 μS·sq and field-effect mobility of ~5 $cm^2/(V·s)$ in the macroscopic channels, which confirm excellent lateral stitching between domains. From transconductance measurements, the intrinsic band gap of GNRs with sub-10 nm widths was estimated as ~80 meV, similar to theoretical expectation. Our method presents a scalable way to fabricate atomically thin elements with 1D characteristics for integration with various nanodevices.

KEYWORDS: graphene nanoribbon, C_{60}, nucleation seed, chemical vapor deposition, large-scale film, electrical conductivity
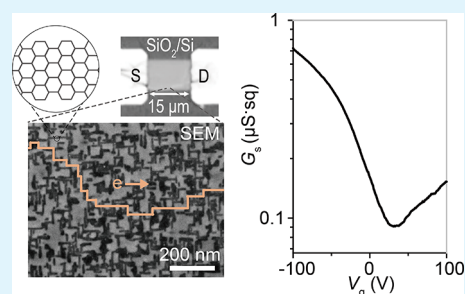
INTRODUCTION

Ultranarrow widths and atomically defined open edges in graphene nanoribbons (GNRs) result in significantly different properties from graphene, suggesting applications in advanced functional nanodevices. Armchair-edge GNRs have characteristic 1D band structures with quantized sub-bands[1] driven by strong quantum confinement across an ultranarrow width. Over a broad energy range, their electronic band gaps are inversely proportional to their widths. In particular, widths <10 nm considerably open the band gap, so GNRs can be used as semiconducting transport elements at room temperature.[1−3] Furthermore, the GNRs can be useful for effective chemical sensing[4] and catalytic activities[5] because the spatially localized electronic states have high electrostatic interactions with nearby substances of molecular-level size, in contrast to 2D graphene sheets, with delocalized states.

Atomically precise structures of GNRs produced by bottom-up synthesis result in excellent electrical properties. However, applications of GNRs require fabrication of GNR films with high electrical conductivity over a large area,[6,7] which has been a difficult task. The main methods that have been used to synthesize the materials are surface polymerization of molecular precursors[8] and chemical vapor deposition (CVD).[9,10] First, surface polymerization leads to dense arrays; however, individual domains are structurally disconnected. A modified method can fuse GNRs into a closely packed array in a small area, but electrical connection across micrometer

ranges has not been reported.[11] Second, CVD on asymmetric surfaces such as Cu(100),[12] Ni(100),[13] and Ge(100)[9,14] leads to bidirectional growth of graphene domains toward orthogonal ⟨110⟩ crystalline orientations as a result of anisotropic interactions between graphene and underlying surfaces. In particular, CVD on Ge(100) yields GNRs with high aspect ratios, up to 70,[15] owing to the large anisotropic interactions between different growth fronts of GNRs and underlying Ge surfaces[16] (see Figure S1 for the detailed discussion). Under a reactive condition, sufficient growth time yields branched GNRs by end-to-side connections among GNRs, so this process suggests a route to form a conducting film over a large scale. However, the density of GNRs (D_{Gr}) is low, usually in a range of 1−10 $\mu m^{−2}$, so the time required for growth of interdomain connections is long, and as a result, the GNRs widen, so they lose their 1D characteristics.

An increase in D_{Gr} is the key to form a GNR grid with ultranarrow widths by CVD on Ge(100). The minimum D_{Gr} to form a grid network has been estimated to be $1/(RW)^2$, where R is the aspect ratio length/width of the GNR and W is the

target width. R as high as ~10 can be readily achieved using feed gases that have a low CH_4/H_2 ratio to change the interfacial energy for each growth front.[15,16] To connect sub-10 nm GNRs that have $R \approx 10$, D_{Gr} should be >100 μm^{-2}, but the low CH_4/H_2 ratio results in extremely incomplete condensation with low D_{Gr},[17] so connections among the sparsely dispersed GNRs do not form readily.

■ RESULTS AND DISCUSSION

Here, we report a simple method to grow conducting GNR grids on centimeter scales. We developed a CVD process that uses solid and gas precursors simultaneously to grow the GNRs on asymmetric Ge(100) surfaces (Figure 1a). Unzipped
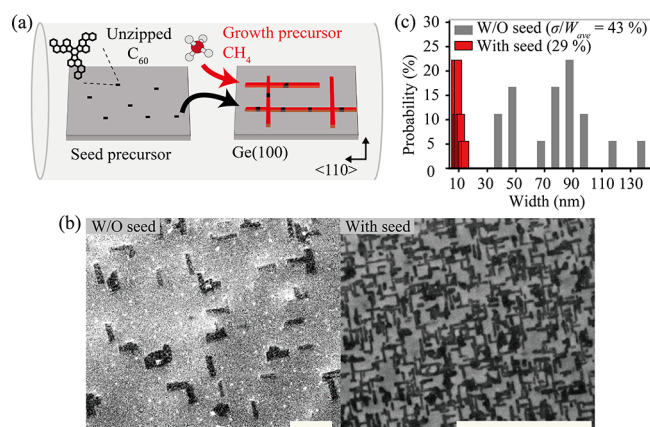

Figure 1. (a) Schematic of nanoscale seed-assisted growth of GNRs. (b) SEM images of as-grown GNRs on Ge(100) substrates without seeds after 45 min growth (left) and with seeds after 9 min growth (right). Scale bar: 500 nm. (c) Width distribution of GNRs with and without seeds (σ: standard deviation, W_{ave}: average width).

fullerene (C_{60}) fragments are sublimated to serve as nanoscale seeds for controlled nucleation, which are critical to form dense, uniform GNRs. Therefore, we can laterally connect individual GNRs of sub-10 nm widths at the nanometer scale over a macroscopic area. The resulting grids are electrically conductive and transferrable and can be patterned for batch fabrication of GNR devices that have semiconducting properties.

The seed precursor must meet two requirements. First, the seeds must be small enough that they do not disturb the ultranarrow widths of GNRs. Second, a substantial amount of seeds must adhere to the growth surface for long enough to nucleate GNR growth. For the fabrication process (Experimental Section and Figures S2−S4), we chose C_{60} as the seeds

because their size is only ~1 nm and they can be deposited as single molecules.[18] The molecules desorb completely at temperatures above ~630 °C because they are spherical and therefore have small contact areas with the substrate.[19] Therefore, after thermal evaporation of C_{60} on a Ge substrate, we annealed C_{60} in H_2 environments (Figure S3) to prompt the adhesion by unzipping the molecules into planar hydrocarbons with increased contact areas. Raman spectra on the samples after the annealing process suggested structural deformations of the deposited C_{60} (Figure S4). Instead of directly placing the seeds on the growth surface, we separately located the seed substrate in the inlet position to minimize formation of surface defects on the growth surface during the unzipping process.

Scanning electron microscopy (SEM) images (Figure 1b) showed that use of the nucleation seeds dramatically increased D_{Gr} and the width uniformity of the GNR arrays. GNRs grown with seeds for 9 min had a D_{Gr} of ~1000 μm^{-2}, which is roughly 200 times higher than ~5 μm^{-2} of samples grown for 45 min without seeds under the same growth condition (see the Experimental Section). Significantly, the D_{Gr} value is substantially higher than a D_{Gr} of ~100 μm^{-2} that is needed to form a GNR grid that has interdomain connections to form percolation pathways over a large area. In addition, the average width W_{ave} was as small as ~7.5 nm with a narrow distribution $\sigma/W_{ave} = 29\%$ in the seed-assisted growth, where σ represents the standard deviation, whereas W_{ave} and σ/W_{ave} were 82 nm and 43% in the reference sample that had been grown without seeds (Figure 1c), respectively.

We discuss why the nanoscale seeds increase the uniformity of W_{ave}. In the reference sample (Figure 1b, left), GNRs with different widths have similar lengths, and the aspect ratio is inversely proportional to the width (Figure S5). Assuming that the length is proportional to the duration of the CVD process after nucleation, the different domains nucleated at the same time, but the anisotropic growth conditions differed significantly among domains, so widths and aspect ratios varied widely. The relative crystallographic orientations between seeds and underlying crystals strongly affect anisotropic growth[15] and thereby determine the aspect ratio. When nucleation is the growth-limiting step, as in the incomplete condensation regime without additional seeds, the nucleation for GNR growth often occurs in uncontrolled defective sites, so the crystallographic orientations of nuclei are randomly oriented with respect to the underlying substrates. As a result, many isotropic domains with small aspect ratios (<2) can be grown (Figure S6). Therefore, the uniform aspect ratios achieved by seed-assisted growth indicate that the introduced
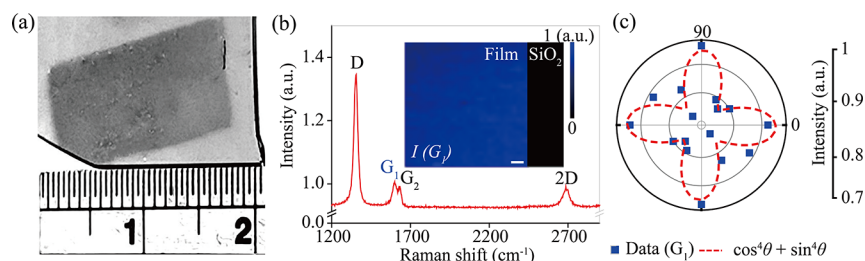

Figure 2. (a) Optical image of the transferred GNR grid on a SiO₂/Si substrate. (b) Raman spectrum of the GNR grid. (Inset) Raman G_1 peak intensity map. Scale bar: 1 μm. (c) Polarization-resolved Raman intensities of G_1 mode for aligned GNR arrays. Red dashed lines: theoretical fitting.
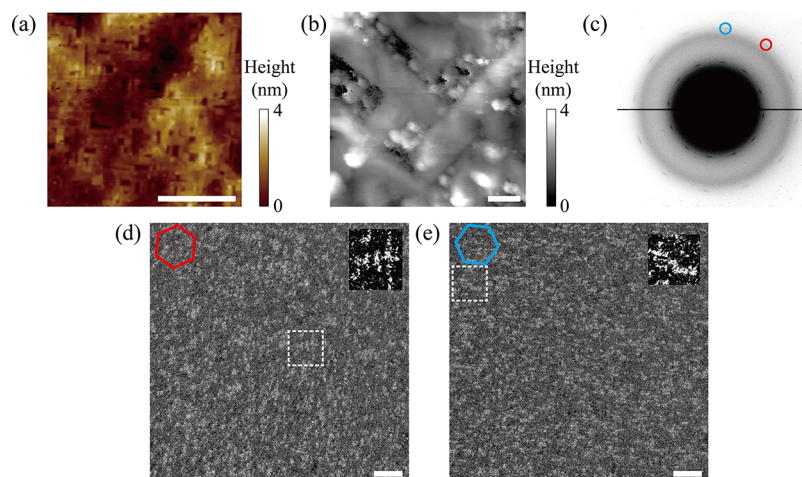
Figure 3. (a) Atomic force microscopy height images of as-grown GNR grids. Scale bar: 200 nm. (b) STM topology image of as-grown GNR grids taken at room temperature with a tip bias of −1 V and tunneling current of 200 pA. Scale bar: 10 nm. (c) SAED of transferred GNR grids by TEM over a 1 μm^2 area. (d, e) Dark-field TEM images with objective aperture filters indicated by colored circles in (c). The insets are zoomed-in images of crystalline domains over the dotted regions, showing a uniaxial alignment in each image. The hexagons on the left, top corners represent the orientations of graphene lattices, as confirmed by SAED. Scale bar: 200 nm.
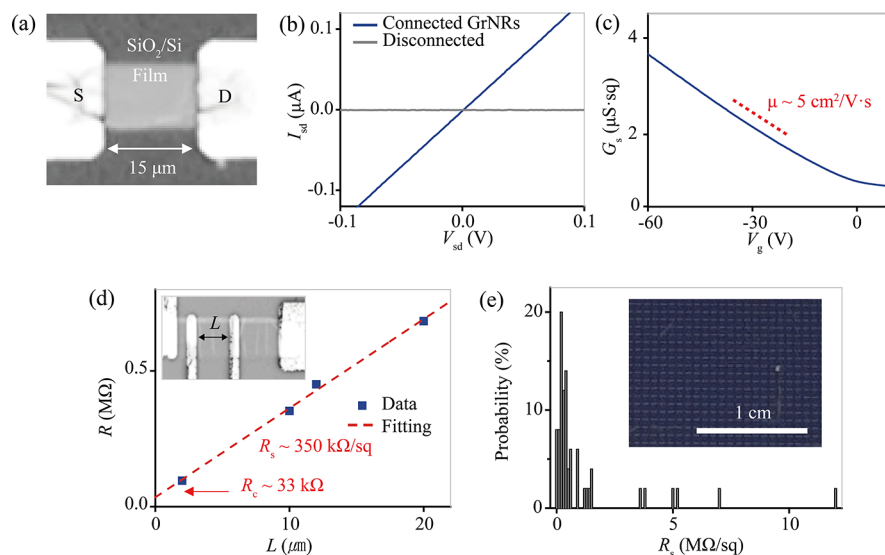

Figure 4. (a) Optical image of a GNR grid channel containing multiple domains, which is sitting on a 100 nm-thick SiO_2/Si substrate. (b) Current−voltage curves for structurally connected (blue line) and disconnected (gray line) GNR grids. The connected GNR grid shows an Ohmic characteristic. (c) Transconductance measurement by back gate sweep with V_{sd} = 0.01 V. The field-effect mobility is calculated assuming that the channel is a continuous film. (d) Transfer length method measurement. (e) Batch fabrication of device arrays and sheet resistance distributions.

nanoscale seeds not only promote nucleation but also provide a defined alignment for growth with uniform aspect ratios.[14]

The uniform, large-scale GNR grids can be transferred onto arbitrary substrates (Figure 2a and Figure S7). The optical absorption measured in GNR grids on a fused silica substrate (Figure S8) was ∼60% of that on a continuous graphene film; this percentage is consistent with the surface coverage, as confirmed in SEM images. Raman spectroscopy on a transferred sample on a SiO_2/Si substrate showed G and 2D peaks that resulted from graphitic carbons (Figure 2b), and the Raman intensity was uniform over the whole transferred area (Figure 2b, inset); this result indicates transfer of uniform grids. Notably, the spectrum shows a strongly increased D peak near 1350 cm^{-1} and nondegenerated G peaks at 1600 and 1623 cm^{-1}. Both features represent the existence of GNRs; the strong D peak is zone-center phonon mode activated in GNRs

with a zone-folding scheme, and the G peak is related to in-plane vibrations that result in broken degeneracy with the anisotropic 1D structure (Figure S9).[20]

The transferred grids were intact, including their macroscopic alignments, which were predominantly aligned along the two perpendicular orientations after growth (Figure 1b). Polarization-dependent G1 peak intensity (Figure 2c) was measured using a configuration of a parallel polarizer and an analyzer (Figure S10a). The peak shows clear polarization dependency; the intensity is the highest when the polarization of incident beams is aligned toward either of the two perpendicular orientations of GNR arrays. The intensity plot follows the equation $\cos^4\theta + \sin^4\theta$ (dashed red line), where θ represents the relative angle between the polarization and the long axis of GNRs. The polarization-dependent signals are expected for two orthogonal 1D nanostructures with strong

depolarization effects for perpendicular polarizations by induced microscopic electric fields in the material.[21,22] This result indicates that the graphitic carbons with planar structures did not exist as impurities, in which Raman signals are polarization-independent (Figure S10b for graphene); as a result, the 1D characteristics are conserved. Data in Figures 1 and 2 indicate that nanoscale-seed-assisted CVD produces transferrable dense and spatially uniform GNR grids.

We further characterized the microstructure of GNRs by using scanning tunneling microscopy (STM) and transmission electron microscopy (TEM) to check the interdomain connectivity and crystalline structures of GNRs. In a dense array of as-grown GNRs (Figure 3a), an STM topology image (Figure 3b) was taken, showing good interdomain connectivity at the nanometer scale. The corresponding differential conductance map (Figure S11), associated with the local density of states, also confirmed homogeneous electrical connections across the junctions between two orthogonally aligned domains. We transferred the sample on a thin supporting membrane (SiN_x of 20 nm) for TEM character-izations. Selected area electron diffraction (SAED) over a 1 μm^2 area show two hexagonal diffraction patterns, rotated by 90°. Dark-field TEM images with objective aperture filters (Figure 3d,e), indicated by colored circles in Figure 3c, show domains of nanoribbon shapes (insets), corresponding to each diffraction spot, demonstrating the high crystallinity of GNRs. Each image shows predominant alignments toward a uniaxial direction. The long axes of GNRs were aligned toward the armchair directions of graphene lattices, implying armchair atomic configurations at the edges. The alignment of GNR edges is consistent with a theoretical prediction[16] and the previously reported experimental data about GNR grown by CVD on Ge(100).[9]

The continuous grid with good interdomain connections enables feasible formation of electrical connections to the film. A standard lithography process is applicable to pattern the channels; GNR grids were transferred onto prepatterned electrodes and then etched into desired shapes (Experimental Section). The number of GNR domains in a channel (N_{domain}) of 15 μm is 300, and the average length of individual GNR domains is ~50 nm (Figure 4a). Even though the current is conducted across many domains, the GNRs show Ohmic behavior with good electrical conduction (Figure 4b). Sheet conductance G_s was deduced from the geometry of the entire channel, including the empty area between GNRs; the average G_s was ~2 $\mu S \cdot sq$. The channels showed clear conductance modulations, as seen in the transconductance curve measured with the bottom gate under ambient conditions (Figure 4c), and showed p-type characteristics at zero gate bias. A maximum field-effect mobility μ of 5 $cm^2/(V \cdot s)$ was estimated using a simple capacitance model $(1/C'_{ox}) \cdot (dG_s/dV_g)$, where C'_{ox} [C/cm^2] represents the areal capacitance between the GNRs and the bottom gate. Both G_s and μ are orders of magnitude larger than the similarly obtained values previously (~few tens nS·sq, ~0.02 $cm^2/(V \cdot s)$) for GNR networks (see Table S1).[23−25]

We tried to further analyze the electrical transports along the percolation pathways. There were roughly maximum 10 percolation pathways observed across a 1 μm width of the channel in SEM images. Considering the measured W_{ave} of 10 nm, a single pathway is estimated to have $G_s \approx 20$ $\mu S \cdot sq$ (10 times the deduced total G_s of the grid). In a polycrystalline graphene film that has excellent lateral stitching with high

angle grain boundaries, the measured interdomain resistivity ρ_{inter} was as low as 500 $\Omega \cdot \mu m$.[26] The series interdomain resistance for a 15 μm-long GNR can be 15 MΩ (= ρ_{inter}/W_{ave} × N_{domain}) for an individual percolation channel, which is significantly lower than the deduced resistance of the channel (~75 MΩ). The limited contribution from ρ_{inter} is distinct from the case in which carrier transports are limited by interdomain hopping.[4,25] In the previous studies, molecular precursors were polymerized from GNR domains with sub-10 nm widths, which were structurally disconnected. The dense arrays of GNRs were stacked together, forming percolation pathways across the overlapped regions of GNRs. However, electrical transports across the weakly connected van der Waals junctions were poor, resulting in low electrical conductivities.

Our GNR grid is uniform on a large scale, so reliable batch fabrication of devices with arbitrary geometry is possible (Figure 4d,e). We performed a transfer length method to check the uniformity and quality of electrical contact. The resistances increased linearly with channel length, with a close fit to 350 kΩ/sq (Figure 4d). The intercept of the line indicated that the contact resistance with the bottom Au electrode was 33 kΩ, which does not dominate the total resistance of the long channel. Considering the contact width between GNRs and electrodes and 1 percolation path/μm, we estimated that the normalized $R_C \approx 330$ $\Omega \cdot \mu m$, which is comparable to the value of optimized contact for graphene.[27] The large-area, uniform grid enables batch fabrication of device arrays (Figure 4e, inset). Over 90% of the devices were electrically conductive without optically visible cracks after the device fabrications, and the distribution of R_s was narrow. These results (Figure 4) together indicate that the GNR grid can form electrical channels across multiple domains with excellent in-plane electrical connectivity and that the GNRs have uniform electrical properties. While there is a finite distribution in R_s, the uniformity can be improved by reducing the doping by contaminants such as hydrocarbons and ionic elements, which were induced nonuniformly from device to device during the device fabrication steps.

The grid of GNRs that have sub-10 nm widths showed distinct electrical properties from bulk graphene. W_{ave} affected the transconductance curves of the GNR grids (Figure 5a and Figure S12). After vacuum annealing, both data showed ambipolar transport with a charge-neutral point (CNP) at a positive gate bias V_g. Significantly, the ratio of the conductance of the on-state and off-state increased as W_{ave} decreased. The conductance is expected to be proportional to W_{ave} and to the
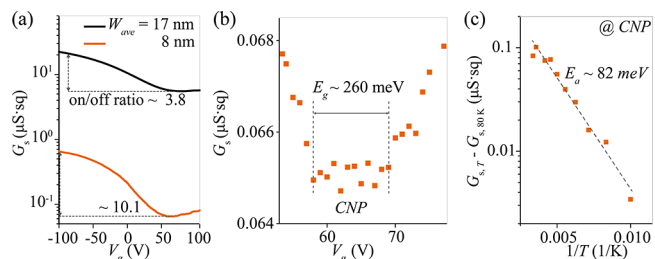

Figure 5. (a) Transconductance curves of two GNR grids with different W_{ave} conducted by back gate sweep with $V_{sd} = 1$ V at room temperature. (b) Conductance minimum near charge neutral point in $W_{ave} = 8$ nm GNR grids. (c) Temperature-dependent $G_{s,T} - G_{s,80K}$ associated with thermally excited carriers (see the Supporting Information for the details).

number of percolation pathways, which change according to growth conditions (see the Experimental Section). Here, the off-state conductance varies more widely between GNRs with different W_{ave} than the on-state conductance; this observation suggests that a factor more than simple geometry affects the minimum G_s. In a GNR grid with W_{ave} = 17 nm, electrical properties were effectively the same as in graphene, which has a negligible band gap. The measured G_s yields an estimated Δn = 25.0 × 10^{11} cm^{-2} using the Drude model (Figure S13), and the sample with W_{ave} = 8 nm had lower Δn = 5.4 × 10^{11} cm^{-2} at CNP. The lower Δn indicates an existence of a finite band gap in the narrower GNR grid.

The sub-10 nm GNR grid showed a differential conductance plateau with dI/dV_g = 0 within a voltage range ΔV_g; this plateau did not occur in data from the reference sample that has W_{ave} > 10 nm (Figure 5b). The transport gap is estimated as 260 meV (see the Supporting Information). As the transport gap is the sum of intrinsic band gap and the electronic potential energy variations that are induced by charge puddles,[28] it represents the upper limit of the intrinsic band gap (Figure S14).[29] We further measured temperature-dependent $G_{s,T}$ at CNP (Figure S15). The activation energy is estimated to be 82 meV from $G_{s,T} - G_{s,80 K}$ (Figure 4c), which represents the $G_{s,T}$ component, associated with only thermally excited carriers (see the Supporting Information). This value is similar to the theoretical expectation for GNRs of sub-10 nm widths.[29] The G_s at CNP is currently limited by extrinsic effects such as surface disorders from the fabrication process,[30] which require further engineering resolve. Still, our data indicate that the electrical properties of GNR grids can be controlled by manipulating their structures.

CONCLUSIONS

In summary, we have realized electrically conductive grids of GNRs with sub-10 nm widths over a large area by devising a nanoscale-seed-assisted CVD method to increase D_{Gr} for interdomain connections. Preparing nanoscale seeds by introducing solid precursors during CVD simplified the previously reported seed-assisted processes, involving epitaxial growth and transfer of graphene and E-beam lithography.[14] The GNR grids can form an important class of nanomaterials to provide unique properties obtained by their mixed dimensionality. They have electrically conducting planar structures in the macroscopic scale, which are ideal to adapt conventional device fabrication techniques for patterning and metallization. On the other hand, their physical properties are determined by the one-dimensional microstructures of GNRs, which confine fundamental objects, such as electrons, heats, and molecules. Properties of GNRs have been intensively studied, but their applications are hampered by difficulty of making device structures on GNRs of short lengths. Our results could pave the way for developing advanced nano-devices based on GNRs by providing films, which are easy to fabricate devices with. We prospect that GNR-based detectors with enhanced sensitivities by ultranarrow widths are particularly promising for realizing functional devices in the near future. Such examples include photodetectors[31] and chemical sensors,[4] which can operate as long as conducting channels exist. In addition, if precise control of edge configurations and defect-free passivation of the edge and surface of large-scale GNR films become possible, then novel quantum devices, which use topological properties associated with the edge states, can be realized for applications.

EXPERIMENTAL SECTION

Seed-Assisted CVD of GNRs. To prepare seed precursors, C_{60} molecules (99.9% powder: 572500, Sigma Aldrich) were deposited by thermal evaporation under high vacuum (1.0 × 10^{-8} Torr) onto Ge(100) substrates at a rate of 0.05−0.1 nm/s at room temperature. After the deposition, the substrate was annealed at 500 °C with H_2 flow (100 sccm) for 12 h to unzip them. Then, the seed substrate was loaded in the inlet position together with growth substrates to prompt nucleation.

GNRs were grown using ambient pressure CVD by a modification of a method reported previously.[9] Ge(100) growth substrates (item #:GeGaa50D05C2R01US, MTI Corporation) were first sonicated for 5 min in acetone and isopropyl alcohol to remove organic residues and then dipped into 20% HF solution for 5 min to etch native oxide. The growth substrate was loaded in a hot-wall quartz tube furnace together with the seed substrate. The furnace was evacuated to 200 mTorr and then filled with Ar (250−300 sccm) and H_2 (100 sccm) to ambient pressure. With constant flow of the Ar and H_2 carrier gases, the temperature was increased to 700 °C and kept there for 2 h. Then, CH_4 (2.5−3 sccm) was introduced, while the temperature was increased to 915 °C in 5 min. The CH_4 flow was maintained for a few minutes at 915 °C. Ar was used as a carrier gas for sublimated seeds, and H_2 suppressed oxidation of the GNRs by the trace amount of oxygen.

The widths of GNRs were affected by the growth conditions. Controlling the growth time is the most obvious way to change the width, but to keep the electrical connection, the growth time must be sufficiently long, so the minimum width in the grid structure increases. An alternative way is to change the aspect ratio of the anisotropic growth rate for GNRs. The final length after lateral fusion is determined by D_{Gr}, but the width can be modulated by changing the aspect ratio of growth rates. The aspect ratio increases as either the partial pressure of CH_4 decreases or the partial pressure of H_2 increases, so we controlled the width by adjusting CH_4 and H_2 contents during growth while maintaining the interdomain connections by ensuring that growth time was sufficient. GNRs were grown using Ar (200 sccm), H_2 (100 sccm), and CH_4 (3 sccm) for 9 min (Figures 1−3); GNRs of W_{ave} = 17 nm were grown using Ar (300 sccm), H_2 (100 sccm), and CH_4 (3 sccm) for 9 min; and GNRs of W_{ave} = 8 nm were grown using Ar (250 sccm), H_2 (100 sccm), and CH_4 (2.5 sccm) for 15 min (Figure 5).

Transfer of GNR Grids. Electrochemical delamination, also known as "bubble transfer", was used to transfer GNR grids.[32] Polymethyl methacrylate (PMMA, 996 K, 8% in anisole) was spin-coated on as-grown substrates at 3000 rpm for 1 min and then baked at 180 °C for 10 min. The PMMA/GNR/Ge(100) sample was placed in 1 M NaOH aqueous solution, and then a bias of 5−15 V was applied across the PMMA/GNR/Ge anode and another Ge cathode to generate H_2 bubbles at the interface between GNR and Ge(100). After delamination, the PMMA/GNR grid floated to the surface of the solution; then, the grid was scooped up and moved to deionized water to clean the surface of the GNR. Finally, the PMMA/GNR grid was scooped up using a target substrate, and PMMA was removed by dipping in acetone for 20 min at 70 °C.

Raman Characterization. Raman spectra were obtained using a homebuilt micro-Raman setup (Figure S10) with an excitation wavelength of 514 nm (0.1−2 mW/cm^2). The excitation laser beams after a linear polarizer were focused using an objective lens (40×, numerical aperture = 0.6) onto samples within a diffraction-limited spot of ∼1.0 μm in diameter. Output signals after an analyzer parallel to the polarizer were guided to a spectrometer equipped with a liquid-nitrogen-cooled charge-coupled detector. To vary the azimuthal angle, we rotated samples by using a rotational mount.

STM Measurements. The samples for STM analysis were prepared by in situ annealing at 400 °C for 2 h under ultrahigh vacuum (UHV) conditions (10^{-10} Torr). We carried out the experiments at room temperature by using a commercial STM (Unisoku, Japan), and we used constant current mode for topography images and simultaneously obtained local density of states (dI/dV)

maps with a lock-in technique with AC modulation (1 kHz, 50 mV). We used an electrochemically etched tungsten tip, which was cleaned by e-beam heating under UHV conditions.

Device Fabrication and Measurement. Metal electrodes (30 nm Au/5 nm Cr adhesion layer) were prepatterned by photolithography on a 300 nm-thick SiO_2/degenerately doped Si substrate. GNR grids coated by PMMA were transferred onto the substrate by electrochemical delamination, and then PMMA was etched using acetone. A protective layer of photoresist (GXR 601) was applied by spin-coating at 4000 rpm for 40 s and then illuminated using a UV source (intensity: 17 W/cm^2) for 2 s to pattern the designed geometry of GNR channels. Air plasma was used to etch the unprotected GNR area for 1 min to define GNR channels.

Electrical characterizations were performed by two probe measurements with modulation of the back-gate voltage V_g. As-fabricated GNR devices originally showed behaviors of hole transport in the transconductance curve within the spanned V_g range (−100 to 100 V), but after vacuum annealing (1.0×10^{-6} Torr, 120 °C, 3 h), they showed ambipolar characteristics at the charge-neutral point (Figure S13). We ascribe the change to the vacuum annealing's efficient removal of water trapped underneath ultranarrow GNRs; water can induce hole doping in a graphene channel.[33] After annealing, data measured under ambient and high-vacuum conditions were almost identical. Data in Figure 5 were taken under vacuum.

■ ASSOCIATED CONTENT

Ⓢ Supporting Information

The Supporting Information is available free of charge at https://pubs.acs.org/doi/10.1021/acsami.1c03437.

> Growth of GNRs on Ge(100) for a high aspect ratio; schematics of seed-assisted growth of GNR grids; morphology of C_{60} on Ge; Raman spectra of pristine and unzipped C_{60}; width and length statics of GNR structures; histogram of aspect ratios for GNRs; transfer by electrochemical delamination; optical absorption spectrum of the GNR grid; nondegenerated, in-plane vibration modes of GNRs; polarization-dependent Raman spectra; differential conductance map of GNR grids; width measurement of GNRs; comparison of electrical properties of GNRs with different widths; estimation of band gap of sub-10 nm GNRs; and list of electrical conductivities of GNR grids (PDF)

■ AUTHOR INFORMATION

Corresponding Author

Cheol-Joo Kim − *Department of Chemical Engineering, Pohang University of Science and Technology, Pohang, Gyeongbuk 37673, Republic of Korea;* ⓞ orcid.org/0000-0002-4312-3866; Email: kimcj@postech.ac.kr

Authors

Namjo Kim − *Department of Chemical Engineering, Pohang University of Science and Technology, Pohang, Gyeongbuk 37673, Republic of Korea*

Shinyoung Choi − *Department of Chemical Engineering, Pohang University of Science and Technology, Pohang, Gyeongbuk 37673, Republic of Korea;* ⓞ orcid.org/0000-0001-5465-7719

Seong-Jun Yang − *Department of Chemical Engineering, Pohang University of Science and Technology, Pohang, Gyeongbuk 37673, Republic of Korea*

Jewook Park − *Center for Artificial Low Dimensional Electronic Systems, Institute for Basic Science (IBS), Pohang 37673, Republic of Korea;* ⓞ orcid.org/0000-0003-3683-1933

Jun-Ho Park − *Department of Chemical Engineering, Pohang University of Science and Technology, Pohang, Gyeongbuk 37673, Republic of Korea;* ⓞ orcid.org/0000-0003-2887-1994

Nguyen Ngan Nguyen − *Department of Chemical Engineering, Pohang University of Science and Technology, Pohang, Gyeongbuk 37673, Republic of Korea*

Kwanghee Park − *Department of Chemistry, Pohang University of Science and Technology, Pohang, Gyeongbuk 37673, Republic of Korea*

Sunmin Ryu − *Department of Chemistry, Pohang University of Science and Technology, Pohang, Gyeongbuk 37673, Republic of Korea;* ⓞ orcid.org/0000-0002-6860-6514

Kilwon Cho − *Department of Chemical Engineering, Pohang University of Science and Technology, Pohang, Gyeongbuk 37673, Republic of Korea;* ⓞ orcid.org/0000-0003-0321-3629

Complete contact information is available at:
https://pubs.acs.org/10.1021/acsami.1c03437

Author Contributions

∥N.K. and S.C. contributed equally to this work. N.K. and C.-J.K. designed the experiments. N.K. and S.C. synthesized GNR samples. N.K., K.P., and S.R. conducted Raman measurements. J.P. conducted STM measurements. N.K., S.C., S.-J.Y., and J.-H.P. conducted device measurements. N.K., S.C., and C.-J.K. carried out data analysis and wrote the manuscript with input from all authors.

Notes

The authors declare no competing financial interest.

■ ACKNOWLEDGMENTS

■ REFERENCES

(1) Son, Y.-W.; Cohen, M. L.; Louie, S. G. Energy Gaps in Graphene Nanoribbons. *Phys. Rev. Lett.* **2006**, *97*, 216803.

(2) Wang, H. S.; Chen, L.; Elibol, K.; He, L.; Wang, H.; Chen, C.; Jiang, C.; Li, C.; Wu, T.; Cong, C. X.; Pennycook, T. J.; Argentero, G.; Zhang, D.; Watanabe, K.; Taniguchi, T.; Wei, W.; Yuan, Q.; Meyer, J. C.; Xie, X. Towards Chirality Control of Graphene Nanoribbons Embedded in Hexagonal Boron Nitride. *Nat. Mater.* **2021**, *20*, 202−207.

(3) Chen, Z.; Narita, A.; Müllen, K. Graphene Nanoribbons: On-Surface Synthesis and Integration into Electronic Devices. *Adv. Mater.* **2020**, *32*, 2001893.

(4) Mehdi Pour, M.; Lashkov, A.; Radocea, A.; Liu, X.; Sun, T.; Lipatov, A.; Korlacki, R. A.; Shekhirev, M.; Aluru, N. R.; Lyding, J. W.; Sysoev, V.; Sinitskii, A. Laterally Extended Atomically Precise Graphene Nanoribbons with Improved Electrical Conductivity for Efficient Gas Sensing. *Nat. Commun.* **2017**, *8*, 820.

(5) Wang, L.; Dong, H.; Guo, Z.; Zhang, L.; Hou, T.; Li, Y. Potential Application of Novel Boron-Doped Graphene Nanoribbon as Oxygen Reduction Reaction Catalyst. *J. Phys. Chem. C* **2016**, *120*, 17427−17434.

(6) Saraswat, V.; Jacobberger, R. M.; Arnold, M. S. Materials Science Challenges to Graphene Nanoribbon Electronics. *ACS Nano* **2021**, *15*, 3674−3708.

(7) Johnson, A. P.; Sabu, C.; Swamy, N. K.; Anto, A.; Gangadharappa, H. V.; Pramod, K. Graphene Nanoribbon: An Emerging and Efficient Flat Molecular Platform for Advanced Biosensing. *Biosens. Bioelectron.* **2021**, *184*, 113245.

(8) Cai, J.; Ruffieux, P.; Jaafar, R.; Bieri, M.; Braun, T.; Blankenburg, S.; Muoth, M.; Seitsonen, A. P.; Saleh, M.; Feng, X.; Müllen, K.; Fasel, R. Atomically Precise Bottom-up Fabrication of Graphene Nanoribbons. *Nature* **2010**, *466*, 470−473.

(9) Jacobberger, R. M.; Kiraly, B.; Fortin-Deschenes, M.; Levesque, P. L.; McElhinny, K. M.; Brady, G. J.; Rojas Delgado, R.; Singha Roy, S.; Mannix, A.; Lagally, M. G.; Evans, P. G.; Desjardins, P.; Martel, R.; Hersam, M. C.; Guisinger, N. P.; Arnold, M. S. Direct Oriented Growth of Armchair Graphene Nanoribbons on Germanium. *Nat. Commun.* **2015**, *6*, 8006.

(10) Oliveira, M. H.; Lopes, J. M. J.; Schumann, T.; Galves, L. A.; Ramsteiner, M.; Berlin, K.; Trampert, A.; Riechert, H. Synthesis of Quasi-Free-Standing Bilayer Graphene Nanoribbons on SiC Surfaces. *Nat. Commun.* **2015**, *6*, 7632.

(11) Jacobse, P. H.; McCurdy, R. D.; Jiang, J.; Rizzo, D. J.; Veber, G.; Butler, P.; Louie, S. G. Z. R.; Fischer, F. R.; Crommie, M. F. Bottom-up Assembly of Nanoporous Graphene with Emergent Electronic States. *J. Am. Chem. Soc.* **2020**, *142*, 13507−13514.

(12) Artyukhov, V. I.; Hao, Y.; Ruoff, R. S.; Yakobson, B. I. Breaking of Symmetry in Graphene Growth on Metal Substrates. *Phys. Rev. Lett.* **2015**, *114*, 115502.

(13) Ago, H.; Tanaka, I.; Ogawa, Y.; Yunus, R. M.; Tsuji, M.; Hibino, H. Lattice-Oriented Catalytic Growth of Graphene Nanoribbons on Heteroepitaxial Nickel Films. *ACS Nano* **2013**, *7*, 10825−10833.

(14) Way, A. J.; Saraswat, V.; Jacobberger, R. M.; Arnold, M. S. Rotational Self-Alignment of Graphene Seeds for Nanoribbon Synthesis on Ge(001) via Chemical Vapor Deposition. *APL Mater.* **2020**, *8*, No. 091104.

(15) Way, A. J.; Murray, E. A.; Göltl, F.; Saraswat, V.; Jacobberger, R. M.; Mavrikakis, M.; Arnold, M. S. Anisotropic Synthesis of Armchair Graphene Nanoribbon Arrays from Sub-5 Nm Seeds at Variable Pitches on Germanium. *J. Phys. Chem. Lett.* **2019**, *10*, 4266−4272.

(16) Dai, J.; Wang, D.; Zhang, M.; Niu, T.; Li, A.; Ye, M.; Qiao, S.; Ding, G.; Xie, X.; Wang, Y.; Chu, P. K.; Yuan, Q.; Di, Z.; Wang, X.; Ding, F.; Yakobson, B. I. How Graphene Islands Are Unidirectionally Aligned on the Ge(110) Surface. *Nano Lett.* **2016**, *16*, 3160−3165.

(17) Venables, J. A.; Spiller, G. D. T.; Hanbucken, M. Nucleation and Growth of Thin Films. *Reports Prog. Phys.* **1984**, *47*, 399−459.

(18) Choi, S.; Nguyen, N. N.; Lee, Y.; Yang, S. J.; Kim, K.; Cho, K.; Kim, C. J. Nanoscale Molecular Building Blocks for Layer-by-Layer Assembly. *Adv. Mater. Interfaces* **2020**, *7*, 2000522.

(19) Wirth, K. R.; Zegenhagen, J. STM Study of the Adsorption of Single C$_{60}$ Molecules on the Ge(111)-c(2 × 8)Surface. *Surf. Sci.* **1996**, *351*, 13−23.

(20) Borin Barin, G.; Fairbrother, A.; Rotach, L.; Bayle, M.; Paillet, M.; Liang, L.; Meunier, V.; Hauert, R.; Dumslaff, T.; Narita, A.; Müllen, K.; Sahabudeen, H.; Berger, R.; Feng, X.; Fasel, R.; Ruffieux, P. Surface-Synthesized Graphene Nanoribbons for Room Temperature Switching Devices: Substrate Transfer and Ex Situ Characterization. *ACS Appl. Nano Mater.* **2019**, *2*, 2184−2192.

(21) Marinopoulos, A. G.; Reining, L.; Rubio, A.; Vast, N. Optical and Loss Spectra of Carbon Nanotubes: Depolarization Effects and Intertube Interactions. *Phys. Rev. Lett.* **2003**, *91*, No. 046402.

(22) Ichida, M.; Mizuno, S.; Kataura, H.; Achiba, Y.; Nakamura, A. Anisotropic Optical Properties of Mechanically Aligned Single-Walled Carbon Nanotubes in Polymer. *Appl. Phys. A: Mater. Sci. Process.* **2004**, *78*, 1117−1120.

(23) Kojima, T.; Nakae, T.; Xu, Z.; Saravanan, C.; Watanabe, K.; Nakamura, Y.; Sakaguchi, H. Bottom-Up On-Surface Synthesis of Two-Dimensional Graphene Nanoribbon Networks and Their Thermoelectric Properties. *Chem. — Asian J.* **2019**, *14*, 4400−4407.

(24) Chen, Z.; Zhang, W.; Palma, C. A.; Lodi Rizzini, A.; Liu, B.; Abbas, A.; Richter, N.; Martini, L.; Wang, X. Y.; Cavani, N.; Lu, H.; Mishra, N.; Coletti, C.; Berger, R.; Klappenberger, F.; Kläui, M.; Candini, A.; Affronte, M.; Zhou, C.; De Renzi, V.; Del Pennino, U.; Barth, J. V.; Räder, H. J.; Narita, A.; Feng, X.; Müllen, K. Synthesis of Graphene Nanoribbons by Ambient-Pressure Chemical Vapor Deposition and Device Integration. *J. Am. Chem. Soc.* **2016**, *138*, 15488−15496.

(25) Richter, N.; Chen, Z.; Tries, A.; Prechtl, T.; Narita, A.; Müllen, K.; Asadi, K.; Bonn, M.; Kläui, M. Charge Transport Mechanism in Networks of Armchair Graphene Nanoribbons. *Sci. Rep.* **2020**, *10*, 1988.

(26) Tsen, A. W.; Brown, L.; Levendorf, M. P.; Ghahari, F.; Huang, P. Y.; Havener, R. W.; Ruiz-Vargas, C. S.; Muller, D. A.; Kim, P.; Park, J. Tailoring Electrical Transport across Grain Boundaries in Polycrystalline Graphene. *Science* **2012**, *336*, 1143−1146.

(27) Wang, L.; Meric, I.; Huang, P. Y.; Gao, Q.; Gao, Y.; Tran, H.; Taniguchi, T.; Watanabe, K.; Campos, L. M.; Muller, D. A.; Guo, J.; Kim, P.; Hone, J.; Shepard, K. L.; Dean, C. R. One-Dimensional Electrical Contact to a Two-Dimensional Material. *Science* **2013**, *342*, 614−617.

(28) Zhang, Y.; Brar, V. W.; Girit, C.; Zettl, A.; Crommie, M. F. Origin of Spatial Charge Inhomogeneity in Graphene. *Nat. Phys.* **2009**, *5*, 722−726.

(29) Han, M. Y.; Brant, J. C.; Kim, P. Electron Transport in Disordered Graphene Nanoribbons. *Phys. Rev. Lett.* **2010**, *104*, No. 056801.

(30) Xue, J. M.; Sanchez-Yamagishi, J.; Bulmash, D.; Jacquod, P.; Deshpande, A.; Watanabe, K.; Taniguchi, T.; Jarillo-Herrero, P.; Leroy, B. J. Scanning Tunnelling Microscopy and Spectroscopy of Ultra-Flat Graphene on Hexagonal Boron Nitride. *Nat. Mater.* **2011**, *10*, 282−285.

(31) Alavi, S. K.; Senkovskiy, B. V.; Hertel, D.; Haberer, D.; Ando, Y.; Meerholz, K.; Fischer, F. R.; Grüneis, A.; Lindfors, K. Photodetection Using Atomically Precise Graphene Nanoribbons. *ACS Appl. Nano Mater.* **2020**, *3*, 8343−8351.

(32) Kim, G.; Jang, A. R.; Jeong, H. Y.; Lee, Z.; Kang, D. J.; Shin, H. S. Growth of High-Crystalline, Single-Layer Hexagonal Boron Nitride on Recyclable Platinum Foil. *Nano Lett.* **2013**, *13*, 1834−1839.

(33) Schedin, F.; Geim, A. K.; Morozov, S. V.; Hill, E. W.; Blake, P.; Katsnelson, M. I.; Novoselov, K. S. Detection of Individual Gas Molecules Adsorbed on Graphene. *Nat. Mater.* **2007**, *6*, 652−655.